Heterogeneity of spiral wear patterns produced by local heating on amorphous polymers

Reginald H. Rice, Enrico Gnecco, William P. King, Robert Szoszkiewicz

Published Version Information

Citation: Rice, R. H., Gnecco, E., King, W. P., & Szoszkiewicz, R. (2013). Heterogeneity of spiral wear patterns produced by local heating on amorphous polymers. Materials Chemistry and Physics, 141(1), 477-481.

Digital Object Identifier (DOI): doi:10.1016/j.matchemphys.2013.05.046

Publisher's Link: http://www.sciencedirect.com/science/article/pii/S0254058413004288

Heterogeneity of spiral wear patterns produced by local heating on amorphous polymers

Reginald H. Rice[1], Enrico Gnecco[2], William P. King[3], Robert Szoszkiewicz[1]

[1] *Department of Physics, Kansas State University, Manhattan, KS 66506-2601, USA*

[2] *Instituto Madrileño de Estudios Avanzados en Nanociencia, Campus Universitario de Cantoblanco, Madrid, Spain*

[3] *Department of Mechanical Science and Engineering, University of Illinois Urbana-Champaign, Urbana, IL 61801, USA*

Abstract

Keywords: nanostructures; polymers; atomic force microscopy (AFM); wear

We report on spiral wear patterns produced at constant angular velocity by hot tip atomic force microscopy (HT-AFM) on surfaces of two common amorphous polymers: polystyrene (PS) and polymethylmethacrylate (PMMA). Topography of these patterns is obtained with regular AFM cantilevers. Topography cross-sections taken from a center of each spiral at a given azimuthal angle Θ relate changes of surface corrugation h_{corr} with tangential velocity v of a thermal cantilever. Polymer wear is characterized by a power law $h_{corr}(v) = \alpha(v/v_{max})^{-\beta}$, which yields a pre-factor α and an exponent β. Below the glass transition temperature T_g, α is polymer specific and β varies weakly between similar conditions and samples. Variations of β are hypothesized to reflect polymer relaxation processes, which are expected to vary only weakly between amorphous polymers. At and above T_g, α approaches initial thermal tip indentation depth within a polymer, β plummets, and a power law relation of h_{corr} with v diverges. These results are explained by heterogeneous wear around T_g due to a local nature of glass transition. At all studied temperatures, additional wear

Email address: rs@phys.ksu.edu (Reginald H. Rice[1], Enrico Gnecco[2], William P. King[3], Robert Szoszkiewicz[1])

heterogeneities are found as due to position on the polymer and Θ. Variations of α and β with position on the polymer are found to be only marginally larger then uncertainties of the thermal tip-polymer interface temperature. Variations of α and β with Θ are found to be largely influenced by buckling of thermal cantilevers traveling in a spiral pattern.

---

1. Introduction

Thin and tailored polymer coatings with enhanced durability are poised to find various applications. Examples include artificial joints, industrial coatings, as well as coatings protecting NEMS and MEMS. Polymers can be synthesized and obtained cheaply in chemical processes scalable to industrial needs. They dissolve readily in various solvents and produce coatings controllable in thickness down to several nanometers via standard spin-coating methods. A wide selection of cross-linking agents is available when a polymer layer interacts too weakly with an underlying substrate. Elastic moduli of polymer films can be tailored between tens of MPa to tens of GPa by UV assisted cross-linking. Finally, chemistry and topography of polymer surfaces can be locally modified *in-situ* with AFM methods [1, 2, 3, 4, 5, 6].

Micro- and nano-scale wear response of any polymer coating is a determining factor for its prolonged functionality, because these local scale changes precede macroscopic failure [7]. Local wear can be understood using linear fracture mechanics, which is not even approximately fulfilled at macroscopic scales, but works for a fully localized process [8, 9]. Nanoscale abrasive wear on polymers has been studied using AFM and hot tip AFM (HT-AFM) methods. The results show abrasive, rippling, tearing, and piling wear modes [10, 11, 12, 7, 3]. Transitions between these regime depend on local force, scan speed, temperature, and brittleness of amorphous polymer samples [10, 11, 12, 13, 3, 7]. However, despite several reports, no explicit correlation between material properties and nano-wear patterns was found on amorphous polymer samples [7]. Therefore, for better understanding of micro- and nano-scale abrasive wear, as well as from

an engineering standpoint, a convenient *in-situ* wear measurement method is needed.

In this paper, a spiral wear pattern is used to study wear on polymers at nano- and micro-scales. A heated AFM cantilever wears surfaces of PS and PMMA films at various tip-sample interface temperatures. A major advantage of local spiral wear patterns lies in fast estimation of material wear and wear heterogeneities. At angular AFM tip velocity of several Hz an area of only about 100 μm^2 and scan times of less than one minute are needed to characterize wear in a range of linear scanning velocities from zero to 50 μm/s. In the case of limited overlap between adjacent tracks of a spiral and at temperatures below T_g, material wear is estimated quantitatively by fitting a power law to the changes of corrugation across spiral pattern vs. an actual thermal tip velocity. At and above T_g, the power law relation breaks down, which is explained by enhanced wear heterogeneities due to a local character of glass transition. Other sources of wear heterogeneities, i.e., depending on a position and a scan direction on a sample, are reported and analyzed too. In particular, wear heterogeneities due to scan direction are influenced by buckling of thermal cantilevers during their spiral trajectory. Beyond various kinds of surface and measurement heterogeneities reported in the article, small fluctuations in the model parameters are likely to originate from the local nature of the viscous flow and plastic deformations and as well as from small deviations from the continuous contact mechanics.

2. Experimental details

The polymers used in this study are PMMA and PS polymers from American Polymer Standards Corporation, with number average molecular weight $M_{w,\mathrm{PS}} = 215.7$ kg mol^{-1} and $M_{w,\mathrm{PMMA}} = 120$ kg mol^{-1}, and polymer polydispersity 1.1. The glass transition temperatures are 95 $\pm$ 5 °C and 105 $\pm$ 5 °C for the PS and PMMA samples, respectively. We note that these are bulk glass transition temperatures, and the glass transition temperatures on the polymer surface depend on load and scanning speed. The PMMA film was produced by spin coating 2.5 % wt polymer solution in chloroform on soda lime fine polished

glass substrate from Fisher Scientific. The PS film was produced by spin coating 2.5 % wt polymer solution in toluene on the same type of glass substrate as the PMMA. In both cases spin coating was done at 500 rpm for 10 s and 2000 rpm for remaining 50 s. HPLC-grade toluene and HPLC-grade chloroform from Sigma-Aldrich were used. The PMMA sample was annealed 15.5 h at 55 °C followed by 1 h at 90 °C. The PS sample was annealed 14 h at 85 °C followed by 2.5 h at 120 °C. The usage of 120 °C, which is above T_g of PS was dictated by an observation that after 14 h at 85 °C PS samples still showed some local pits. A resulting film thickness of 240 ± 60 nm for PMMA and 220 ± 50 nm for PS films were determined by a scratch test with AFM.

Thermal cantilevers are AFM cantilevers with integrated heaters [14, 15, 16]. They were mounted in a di-CP-II AFM system equipped with a module to read their temperature [1, 3]. The tip temperature calibration was based on acquiring indentation profiles on two polymer samples with known softening temperatures [15, 1, 16]. The elastic spring constants of thermal cantilevers were obtained using the thermal noise method [17] to be between 0.5-0.7 N/m. The tip of a thermal cantilever, which produced the reported here spirals and measured using SEM, had a radius of $R_y = 170 \pm 10$ in the longitudinal direction and $R_x = 120 \pm 10$ nm in the transverse direction.

Assuming that the radial distance r of the spiral grows linearly with the time t as $r(t) = At$, and that the angular velocity ω is constant, the linear velocity v of the thermal tip grows with r as $v = \sqrt{A^2 + (\omega r)^2}$. This dependence becomes almost linear, and the velocity almost tangential, when $r \gg A/\omega$, which is the case for all spiral windings, except the very first one, in the presented data.

The AFM topographs of the polymer films with the spirals were recorded in contact mode with Proscan software and SiN_x MLCT-F cantilevers, all from Bruker USA. The MLCT-F cantilevers had a nominal elastic spring constant between 0.3 to 1 N/m and nominal curvature radii below 20 nm.

3. Results and discussion

Figure 1.A. shows an AFM topograph of a typical spiral wear pattern generated on a PS sample via the HT-AFM method. The spiral pattern was made with a cantilever heated such that the tip-sample interface was at 89 ± 12 ^{0}C. Amplitude of indentation profiles presented in the inset of Fig. 1.A. decreases with the scan speed quickly. To quantify the amplitude decrease, surface corrugation is calculated as maximum amplitude difference between the bottom of each trough and any of its two sides.

As observed particularly well in the centers of each spiral, the longer a thermal AFM tip resides in a given spot on the surface, the more damage is caused. Thus, a $1/v$ - like dependence of corrugation is expected unless the scan velocity is low enough that no plastic indentation is made. However, the $h_{corr}(v) = a(v/v_{max})^{-1}$ relation does not fit our experimental data. We suggest that visco-plastic indentations and surface heterogeneities produce a spread in the characteristic timescales associated with the surface plowing wear observed in our experiments. Thus, we propose to use a power law. Our rationale is that a power law description explained the spread in shear stress relaxation times and a spread in dynamic surface structure factors obtained from the scattering experiments on amorphous polymers below their glass transitions [19, 20]. Consequently, in the analysis below, velocity dependence of the spiral corrugation profiles $h_{corr}(v)$ is fitted by a following equation:

$$h_{corr}(v) = \alpha(v/v_{max})^{-\beta}. \quad (1)$$

Here, the normalizing velocity v_{max} is the velocity of the cantilever at the last winding of a spiral, α is constant, and β is an arbitrary exponent. Extensive gallery of corrugation profiles fitted with Eq. 1 in the case of spirals obtained at various positions and at various tip-sample interface temperatures is presented in the Suppl. Materials.

Making of each spiral starts after a hot thermal tip resides in its center for at least several seconds. This is much longer than in any other point along its

spiral trajectory. Thus, the corrugation plots like in Fig. 1.B are fitted after rejecting the first point.

Table 1 reports the values of $\log(\alpha)$ and β obtained in a range of temperatures for several spirals on PS and PMMA. For each spiral at least four distinct cross-section profiles were fitted and the results were averaged. Statistical significance of the values of $\log(\alpha)$ and β has been addressed in detail in the Supplementary Materials. When overlap between adjacent tracks is small and temperatures are below the glass transition temperature, Eq. 1 fits the data very well, i.e., with an absolute value of linear correlation coefficients R_{corr} of 0.9 and more, see the Suppl. Materials. At temperatures below the polymer softening, and up 30 % overlap between windings, the values of α are distinctively different between PS and PMMA, while the values of β are nearly constant. For up to 30 % overlap between the consecutive windings measured values of β are close to an exponent of 0.6, which was calculated by Roe et al. [21] in molecular dynamics simulations of the structure factor relaxation of the polymer chains below the T_g. Thus, arguably nano-wear below glass transition of amorphous polymers follows a similar power law as universal relaxation phenomena in glasses [19, 20].

At tip-surface temperature close or surpassing T_g Eq. 1 fails as quantified by $|R_{corr}| < 0.7$. Consequently, the values of α approach initial indentation depths at these conditions, and the values of β drop precipitously. These results are similar to the observations of Keddie et al. [22]. Keddie et al. successfully described dependence of T_g on the polymer film thickness by suggesting that at the surface of a glassy polymer a liquid-like layer exists whose size is described by a power law. The power law was found to diverge when the glass transition was approached from below. Divergence of the power law did not depend strongly on the molecular weight of the polymer. Similarly, if wear is described by a power law at temperatures below T_g, then such a power law is expected to diverge above T_g due to percolation of local heterogeneities. Furthermore, the divergence should not depend strongly on the type of a given amorphous polymer. This is exactly the behavior observed here. Below T_g a power law fits the corrugation profiles very well, and it breaks above T_g due to too much

sample	t_{sample} (°C)	log(α) α in (nm)	β	corr. coeff.	overlap %
PMMA	84 (11)	0.48 (0.32)	0.60 (0.19)	0.86	20
	89 (12)	0.74 (0.37)	0.89 (0.43)	0.93	10
	97 (12)	1.09 (0.14)	0.71 (0.26)	0.93	15
	97 (12)	2.00 (0.18)	0	0.32	100
	113 (14)	2.02 (0.16)	0	0.16	100
(*)	97 (12)	1.40 (0.47)	0.65 (0.46)	0.88	10
PS	89 (12)	1.67 (0.40)	0.54 (0.40)	0.83	75
(*)	97 (12)	1.70 (0.44)	0.68 (0.46)	0.96	30

Table 1: The results of corrugation vs. AFM cantilever velocity obtained from a linear fit to the function $\log[h_{corr}(v)] = \log(\alpha) - \beta * \log[v/v_{max}]$ like in Fig. 1.B. At least four profiles are averaged for each spiral. The spirals have either 300 nm and 600 nm (denoted by (*)) spacing between windings. The studentized errors are presented in brackets e.g., 1.7 (0.4) means 1.7 $\pm$ 0.4. The values of $\beta = 0$ in the 4th and 5th data rows reflect the fact that experimentally obtained values of β did not pass statistical criterion for non-zero slope. See the Supplementary Materials for detailed calculations.

overlap between windings of the spirals. One might hypothesize that such a behavior is caused by a liquid layer of an amorphous polymer spreading out.

Indeed, spreading out of a liquid layer can be interpreted as an enhanced viscous matter flow during the polymer wear process above T_g. Thermal stabilization of the polymers has been showed to occur at the time scales of less than 1 μs and AFM tip-polymer contact radii are of the order of only tens of nanometers below the T_g [23]. At such conditions, plastic deformations and/or viscous matter flow do not affect the consecutive spiral windings. However, the situation changes above the T_g. There, due to significant decrease of the Young modulus of the amorphous polymers above the T_g [24], the length scale associated with plastic polymer deformations and a viscous matter transport around the wearing scar become comparable with the spacing between windings used in our experiment. Then, our model is expected to break down, and the correlation coefficients are expected to drop.

Overall, in the case of limited overlap between windings and temperatures below T_g, the values of a pre-factor α in Table 1 provide a quantitative measure of local wear at given loads and tip-sample surface temperatures. However, notable errors of α and β point out towards some intrinsic wear heterogeneity

at all studied temperatures.

Despite preparing uniform polymer films, some wear heterogeneity with sample position is expected. Three spirals obtained in the same conditions, but at different positions on the polymer, were fitted with Eq. 1 to four corrugation profiles for each spiral as in Fig. 1. Errors of 20 - 40 % in α and β were obtained, despite negligible surface wear induced in rescans of the spirals with a regular cantilever. See the Suppl. Data. Errors in α and β are contrasted with 20 - 30 % uncertainties of thermal AFM tip - polymer interface temperature, which are currently unavoidable. In consequence, wear heterogeneity depending on the position on a polymer is at most only marginally larger than spatial heterogeneity provoked by a spread in surface temperature estimates.

The values of α and β were found to depend on an azimuthal angle Θ across a spiral. Fig. 2 plots changes of α and β along 18 profiles taken across the spiral from Fig. 1 with a Θ step of 20 degree. A quasi-harmonic dependence of α and β on Θ and their respective 180 degree phase shift is clearly visible there. We note that rotating the sample did not remove these heterogeneities. Those results point towards buckling of a thermal AFM cantilever during making of a spiral. In the experimental configuration, the longitudinal direction of a thermal cantilever modifying the sample is along $\Theta = 90$ degree. Thus, most of cantilever buckling is expected in the vicinity of 0 and 180 degrees of Θ. Approximating a thermal cantilever as a rectangular cantilever, its buckling spring constant, k_b is estimated as $k_b = (2Lk_z)/(3h_t)$. Here, k_z is a normal spring constant of this cantilever, L is the cantilever's length, and h_t is the tip's height [25]. A value of $L = 150 \pm 20$ μm was estimated from optical microscope observations, and a value of $h_t = 1.2 \pm 0.1$ μm was estimated from SEM. Using a typical value of $k_z \simeq 0.5$ N/m one obtains $k_b = 42 \pm 9$ N/m. Large value of k_b would produce small, but yet noticeable, changes in the overall normal force detected by the AFM system during cantilever's buckling.[1] Thus, despite a beneficial

[1] Torsional elastic spring constant of the thermal cantilevers is yet a few times larger than its buckling spring constant and it couples significantly less with the normal force measurements than a buckling spring constant does.

low AFM feedback used during a thermal modification process, buckling of a thermal cantilever in vicinity of 0 and 180 degrees of Θ, results in larger than typical polymer indentations and wear, and particularly at low sliding velocities. Consequently, steeper linear fits of Eq. 1 to the corrugation profiles are produced, which means increased values of β. Increasing β produces a decrease in $\log(\alpha)$ intercepts, which qualitatively explains the experimental data in Fig. 2 remarkably well. However, from the collected data it is difficult to elucidate quantitatively which per cent of the reported variations of α and β with Θ relates to buckling of a thermal cantilever, and which per cent might indeed show polymer dependent wear heterogeneity with Θ. Clearly, to minimize interference of wear processes with elastic properties of the thermal AFM cantilever, any wear parameters should be calculated from the cross-sections in the vicinity of Θ of 90 or 270 degrees.

4. Conclusions

In conclusion, spiral wear patterns obtained using the HT-AFM method reported on wear properties and wear heterogeneities on amorphous polymers. Corrugation profiles taken along the spirals as a function of tangential velocity of a thermal tip were fitted with a power law. The power law relation provided a pre-factor α and a power law exponent β. In the case of limited overlap between adjacent tracks of a spiral and at temperatures below T_g, the power law provided an excellent agreement with the experimental data, e.g., with fit correlation coefficients of 0.9 or more. In this case, the value of α varied significantly with temperature, which was used as a quantitative measure of wear. At these conditions, the values of β varied weakly with temperature and between samples. It was hypothesized that weak variations of an exponent β below T_g reflected polymer relaxation phenomena, which were similar between amorphous polymers. If this is correct, significant variations of β are expected below T_g for semi-crystalline polymers [19, 20], which remains to be tested.

A major limitation of our derivations is to describe the polymer wear well above the T_g. Power law fits of corrugation profiles with tip velocity diverged at

temperatures at and above T_g, as assessed through the low values of the correlation coefficients between the data and the fits. Power law divergence signified substantial wear heterogeneities, which were explained as due to a local nature of glass transition. Beyond that, wear heterogeneities due to position on a sample and wear direction were reported. Wear heterogeneities with the position on a polymer sample were only marginally larger than wear uncertainties provoked by errors in calculating tip-sample interface temperature. Wear heterogeneities due to azimuthal wear direction correlated with buckling of thermal cantilevers traveling in a spiral pattern. Beyond various kinds of surface and measurement heterogeneities reported in the article, additional fluctuations in the model parameters are likely to originate from the local nature of the viscous flow and plastic deformations, as well as from small deviations from the continuous contact mechanics [9]. Overall, our current model has captured the key and intrinsic features of local polymer wear under local heating and up to vicinity of a glass transition temperature. More advanced theoretical and computational studies are needed to obtain a more comprehensive description. Due to complexity of the temperature dependent viscous flow at length scales comparable to mean gyration radii of the polymers the coarse grained molecular dynamics studies are envisaged to be a good start.

The results obtained in this paper are useful for quantitative nanoscale characterization of temperature wear on amorphous polymers. On one hand, the use of an Archimedean spiral instead of a circle (like in pin-on-disk macro-tribological tests) or a straight line is quite original. Only thanks to this scan pattern we could investigate the abrasive process for continuously varying velocity values. On the other hand, we have introduced a reasonable and not trivial data fit based on the power law function which, according to our knowledge has not been directly applied to study polymer wear in previous works. We showed that for low degree of overlap between consecutive windings our data are very reproducible and able to differentiate between wear properties of PMMA and PS. As such, a new technique with a theoretical background has been established for local wear testing. Our results are also expected to be of considerable

interest for future modeling of plastic deformation of polymer surfaces initiated by local heat and load.

Acknowledgments

Discussions with Dr. Reinhold Wannemacher from IMDEA Institute are greatly appreciated.

5. Figure Captions

Figure 1. (A) An Archimedean spiral on PS made with a hot tip AFM with a normal force $F_N = 20 \pm 5$ nN and an angular velocity $\omega = 3.14$ s^{-1}. This topography rescan was obtained in a contact mode AFM using MLCT-F lever from Bruker at load of 15 ± 3 nN. Four cross-sections are marked. (B) Two selected corrugation profiles plotting decimal logarithm of the corrugation h_{corr} between troughs plotted against decimal logarithm of a ratio of an actual tip velocity v over v_{max}, see text.

Figure 2. (A) A spiral illustrated in Fig. 1 with 18 cross-sections out of which corrugation profiles were calculated. (B) A systematic plot of the values of α and β obtained after fitting Eq. 1 to the corrugation profiles. Note ascending values of $\log(\alpha)$ and descending values of β.

[1] R. Szoszkiewicz, T. Okada, S. C. Jones, T. D. Li, W. P. King, S. R. Marder, and E. Riedo, Nano letters 7 (2007) 1064 – 1069.

[2] D. B. Wang, R. Szoszkiewicz, M. Lucas, E. Riedo, T. Okada, S. C. Jones, S. R. Marder, J. Lee, and W. P. King, Appl. Phys. Lett. 91 (2007) 243104.

[3] E. Gnecco, E. Riedo, W. P. King, S. R. Marder, and R. Szoszkiewicz, Phys. Rev. B 79 (2009) 235421.

[4] D. Pires, J. L. Hedrick, A. De Silva, J. Frommer, B. Gotsmann, H. Wolf, M. Despont, U. Duerig, and A. W. Knoll, Science 328 (2010) 732 – 735.

[5] H. M. Saavedra, T. J. Mullen, P. P. Zhang, D. C. Dewey, S. A. Claridge, and P. S. Weiss, Rep. Progr. Phys. 73 (2010) 036501.

[6] J. Duvigneau, H. Schonherr, and G. J. Vancso, ACS Nano 4 (2010) 6932 – 6940.

[7] A. Dasari, Z.-Z. Yu, and Y.-W. Mai, Mat. Sci. Eng. R (2009) 31 – 80.

[8] M. Raab and E. Nezbedova, in: Hanser (Ed.), Toughness of ductile polymers, 2000, chapter 3.

[9] B. Luan and M. O. Robbins, Nature 435 (2005) 929 – 932.

[10] R. H. Schmidt, G. Haugstad, and W. L. Gladfelter, Langmuir 19 (2003) 10390 – 10398.

[11] R. H. Schmidt, G. Haugstad, and W. L. Gladfelter, Langmuir 19 (2003) 898 – 909.

[12] B. Gotsmann and U. Duerig, Langmuir 20 (2004) 1495 – 1500.

[13] W. Brostow, H. E. H. Lobland, and M. Narkis, J. Mater. Res. 21 (2006) 2422 – 2428.

[14] P. Vettiger, M. Despont, U. Drechsler, U. Durig, W. Haberle, M. I. Lutwyche, H. E. Rothuizen, R. Stutz, R. Widmer, and G. K. Binnig, IBM J. Res. Dev. 44 (2000) 323 – 329.

[15] J. Lee, T. Beecham, T. L. Wright, B. A. Nelson, S. Graham, and W. P. King, J. Microel. Sys. 15 (2006) 1644 – 1648.

[16] B. A. Nelson and W. P. King, Sens. Act. A: Phys. 140 (2007) 51 – 59.

[17] A. Dey and R. Szoszkiewicz, Nanotechnology 23 (2012) 175101.

[18] E. Gnecco, R. Bennewitz, and E. Meyer, Phys. Rev. Lett. 88 (2002) 215501.

[19] J. C. Phillips, Rep. Progr. Phys. 59 (1996) 1133 – 1207.

[20] E.-J. Donth, in: The glass transition: relaxation dynamics in liquids and disordered materials. Springer-Verlag, Berlin, 2001.

[21] R. J. Roe, J. Non-cryst. Sol. 77 (1994) 172 – 174.

[22] J. L. Keddie, R. A. L. Jones, and R. A. Cory, Europhys. Lett. 27 (1994) 59 – 64.

[23] R. H. Rice, P. Mokarian-Tabari, W. P. King, and R. Szoszkiewicz, Langmuir 28 (2012) 13503 – 13511.

[24] S. K. Kaliappan, B. Cappella, Polymer 46 (2005) 11416 - 11423.

[25] M. Labardi, Nanotechnology 18 (2007) 395505.

Figure 1.

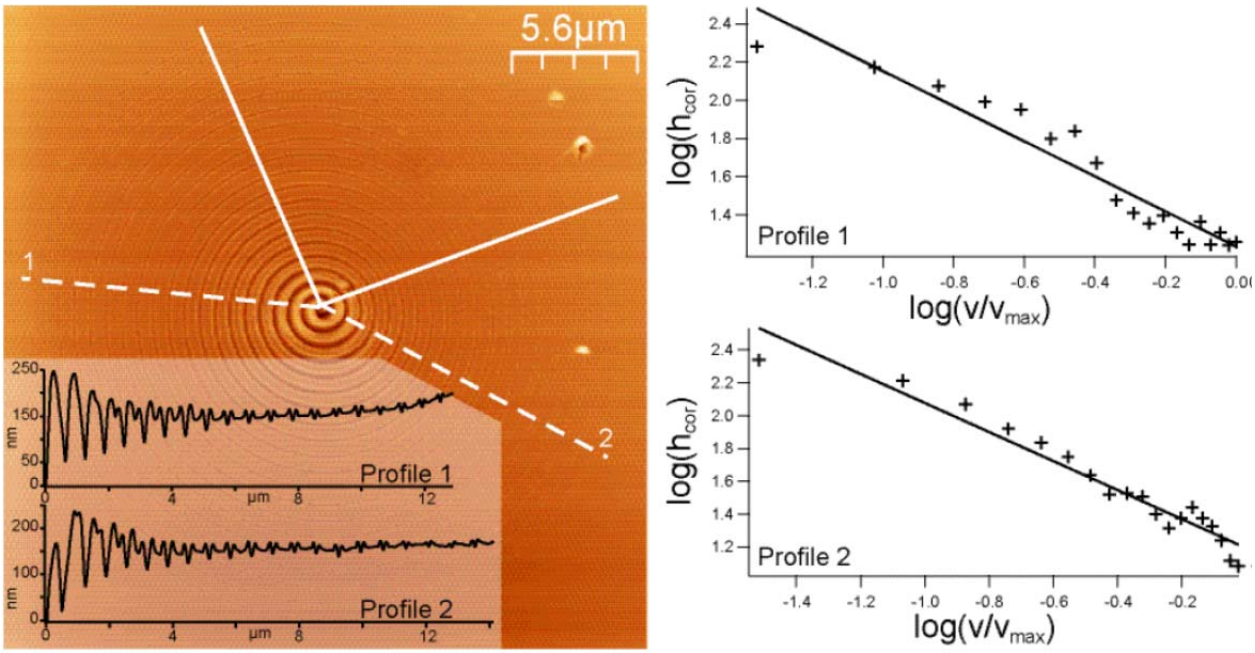

Figure 1. (A) An Archimedean spiral on PS made with a hot tip AFM with a normal force $F_N = 20 \pm 5$ nN and an angular velocity $\omega = 3.14$ s^{-1}. This topography rescan was obtained in a contact mode AFM using MLCT-F lever from Bruker at load of 15 ± 3 nN. Four cross-sections are marked. (B) Two selected corrugation profiles plotting decimal logarithm of the corrugation h_{corr} between troughs plotted against decimal logarithm of a ratio of an actual tip velocity v over v_{max}, see text.

Figure 2.

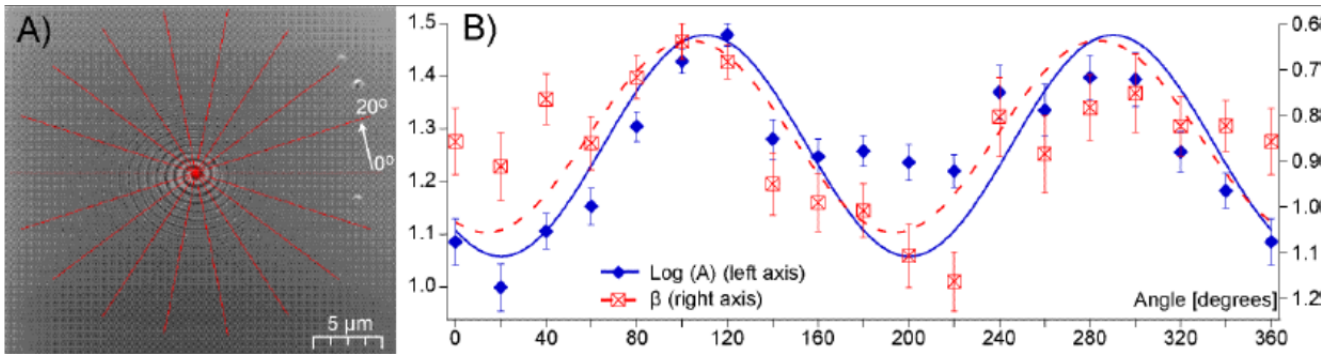

Figure 2. (A) A spiral illustrated in Fig. 1 with 18 cross-sections out of which corrugation profiles were calculated. (B) A systematic plot of the values of α and β obtained after fitting Eq. 1 to the corrugation profiles. Note ascending values of $\log(\alpha)$ and descending values of β.

Supplementary Materials for the manuscript: "Heterogeneity of spiral wear patterns produced by local heating on amorphous polymers" by R. Rice et al.

This file includes:

- Calculations of mean gyration radii, R_G, for used here polymers.
- Gallery of corrugation profiles fitted with a power law on the spirals reported in the Table 1 in the main paper, Figs. S1 to S8.
- Effects of multiple rescans of the same spiral with a regular AFM cantilever, Fig. S9.
- Spatial heterogeneity of the corrugation profiles on PMMA and PS, Figs. S10 and S11.

- **Calculations of R_G**
  Mean gyration radius R_G is calculated using a standard formula: $R_G = b*(Z/6)^{0.5}$. Here: b is the Kuhns length, and Z is the degree of polymerization of each polymer. The value of b for PS is 0.7 nm (J. K. Kim and C. D. Han, in Polymer Materials: Block-Copolymers, Nanocomposites, Organic/Inorganic Hybrids, Polymethylenes, edited by K. S. Lee and S. Kobayashi (2010), Vol. 231, pp. 77-145.).
  The value of b for PMMA is 1.4 nm (J. E. Mark, Physical Properties of Polymers Handbook; AIP Press. Woodbury, New York, 1996).
  Mw of our PS sample is 215,700 g/mole, which corresponds to Mn=196,091 g/mole, when using a polydispersity index of 1.1 as provided by manufacturer. Mn of each PS monomer is 104 g/mole.
  Mw of our PMMA sample is 120,000 g/mole, which corresponds to Mn=109,091 g/mole, when using a polydispersity index of 1.1 as provided by manufacturer. Mn of each PMMA monomer is 100 g/mole.
  Thus, the respective degrees of polymerizations $Z = Mn_{polymer}/Mn_{monomer}$ are 1885 for PS and 1091 for PMMA.

Figures S1 to S8 show corrugation profiles and least-squares linear regression fits of the power law relation, i.e., $\log[h_{corr}(v)] = \log(\alpha) - \beta * \log[v/v_{max}]$, to the corrugation profiles along the spirals. Six examples for PMMA and two examples for PS are produced, which corresponds to the data reported in the Table 1 of the paper. For example, Fig. S1 refers to the first data row within the Table 1, i.e., the data for PMMA at 84 $\pm$ 11 ^{o}C on the polymer surface. Similarly, Fig. S2 refers to the second data row within the Table 1, i.e., the data for PMMA at 89 $\pm$ 12 ^{o}C on the polymer surface. Reported errors of the fit parameters are their standard deviations. Abs(V_{Pr}) is an absolute value of a linear correlation coefficient.

Using the data reported in Figures S1 to S8 a following statistical analysis is performed. First, we test statistical significance of the slope and intercept, i.e., the values of β and $\log(\alpha)$ reported in the Table 1. A t-Student test is used to test a statistical hypothesis H_0 such that $\log(\alpha) = 0$ or $\beta = 0$ (Bevington, P.R., Data reduction and error analysis for the physical sciences, McGraw-Hill Book Company, New York 1969). To do so a calculated t-Student coefficient for each slope and intercept has been compared with its tabulated value for a given number of degrees of freedom and at a 90 % confidence level. For example, in the case of the first corrugation profile in Fig. S1, we got a value of $\log(\alpha) = 0.216$ and its standard deviation $s_{\log(\alpha)} = 0.035$. Thus, a calculated value for a t-Student coefficient is $t_{\log(\alpha)} = \log(\alpha)$ / $s_{\log(\alpha)} = 6.17$. This value is much larger then a tabulated value of t-Student coefficient $t_{16,0.10} = 1.75$ read from the statistical tables for 16 degrees of freedom of the studied case (Bevington, P.R., Data reduction and error analysis for the physical sciences, McGraw-Hill Book Company, New York 1969). Thus, H_0 is not true in this case. By extending this analysis to all reported values of $\log(\alpha)$ and β, it has been found that H_0 holds only for the values of β in the case of 100 % overlap between consecutive windings, i.e., for the data reported in Figures S4 and S5 and in the rows 4th and 5th within Table 1.

Second, we test whether the values of $\log(\alpha)$ and β obtained for different experimental conditions are statistically different. To do so, we studentize standard deviations of those parameters to calculate their confidence intervals. For example, in the case of the first corrugation profile in Fig. S1, a studentized error of $\log(\alpha)$ at 90% confidence limits is $t_{16,0.10} * s_{\log(\alpha)}$= 1.75*0.035 = 0.061. This analysis is extended to all data, and studentized errors of $\log(\alpha)$ and β are now reported in the Table 1. We conclude that even within those errors, the observed differences in polymer behavior below and in a close proximity of the glass transition temperature are statistically significant.

Image	Material	R [µm]	T_{tip} [°C]	T_{surf} [°C]	T_{surf} Error	Profile #	overlap	Log (A)	Log (A) Error	-β	-β Error	V_Pr	Abs(V_Pr)
8DEC_DD	PMMA	6	164	84.4	11.5	1	20%	0.21605	0.0352	-0.76457	0.06	-0.953926	0.953926
8DEC_DD	PMMA	6	164	84.4	11.5	2	20%	0.65543	0.0559	-0.52834	0.09	-0.810501	0.810501
8DEC_DD	PMMA	6	164	84.4	11.5	3	20%	0.4069	0.0505	-0.61055	0.09	-0.845627	0.845627
8DEC_DD	PMMA	6	164	84.4	11.5	4	20%	0.62423	0.053	-0.4916	0.09	-0.814035	0.814035
						AVERAGE	20%	0.48	0.18	-0.60	0.11	-0.86	0.8560223

Note: Each plot below has left axis of log(h_{cor}) and bottom axis of log(v/v_{max})

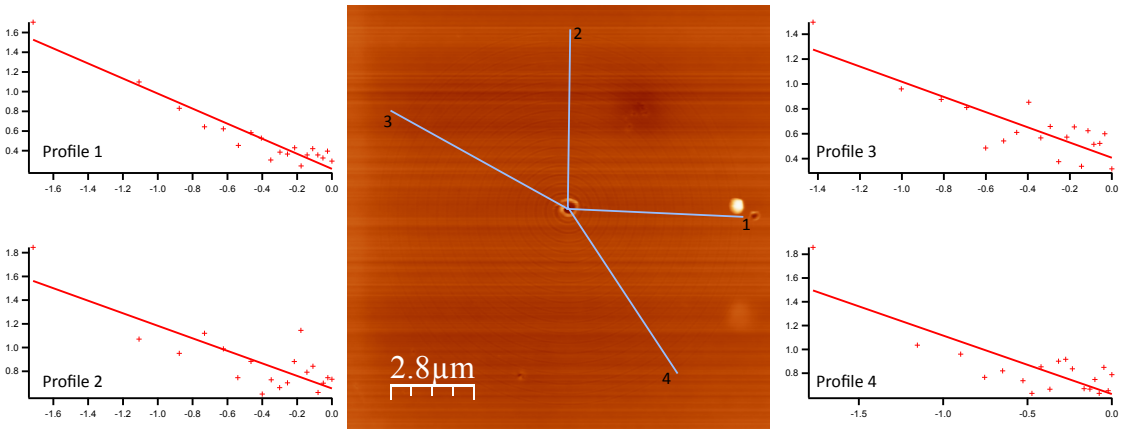

Figure S1. The data reported in a first data row of the Table 1 in the paper: PMMA heated at 84 ± 11 ^{o}C on the polymer surface.

Image	Material	R [µm]	T_{tip} [°C]	T_{surf} [°C]	T_{surf} Error	Profile #	overlap	Log (A)	Log (A) Error	-β	-β Error	V_Pr	Abs(V_Pr)
30DEC_71	PMMA	6	186	88.7	11.8	1	5%	0.51238	0.0482	-1.0313	0.1	-0.928297	0.928297
30DEC_71	PMMA	6	186	88.7	11.8	2	10%	0.96403	0.0383	-0.62501	0.06	-0.923283	0.923283
30DEC_71	PMMA	6	186	88.7	11.8	3	5%	0.79047	0.0387	-0.79105	0.07	-0.936797	0.936797
30DEC_71	PMMA	6	186	88.7	11.8	4	10%	0.67501	0.0454	-1.101	0.1	-0.941728	0.941728
						AVERAGE	8%	0.74	0.23	-0.89	0.26	-0.93	0.9325263

Note: Each plot below has left axis of $\log(h_{cor})$ and bottom axis of $\log(v/v_{max})$

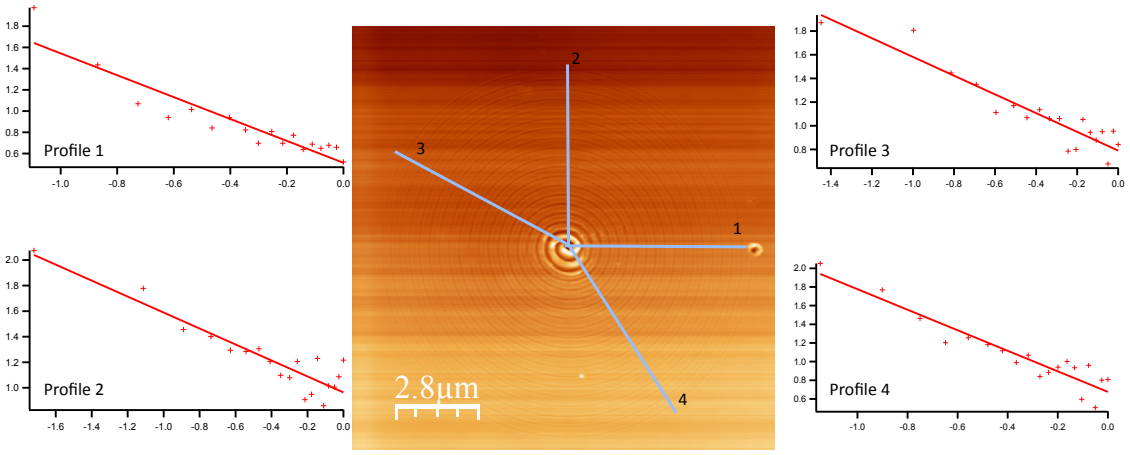

Figure S2. The data reported in a second data row of the Table 1 in the paper: PMMA heated at 89 ± 12 °C on the polymer surface.

Image	Material	R [μm]	T_{tip} [°C]	T_{surf} [°C]	T_{surf} Error	Profile #	overlap	Log (A)	Log (A) Error	-β	-β Error	V_Pr	Abs(V_Pr)
8DEC_D1	PMMA	6	206	97	12.5	1	5%	0.95004	0.0501	-0.71164	0.09	-0.896355	0.896355
8DEC_D1	PMMA	6	206	97	12.5	2	10%	1.1649	0.0348	-0.55998	0.07	-0.890644	0.890644
8DEC_D1	PMMA	6	206	97	12.5	3	25%	1.1737	0.0414	-0.75737	0.08	-0.913894	0.913894
8DEC_D1	PMMA	6	206	97	12.5	4	10%	1.1276	0.0192	-0.57721	0.04	-0.967358	0.967358
8DEC_D1	PMMA	6	206	97	12.5	5	20%	1.0318	0.0358	-0.90026	0.07	-0.949599	0.949599
8DEC_D1	PMMA	6	206	97	12.5	6	10%	1.1032	0.0338	-0.7628	0.07	-0.941981	0.941981
						AVERAGE	13%	1.09	0.08	-0.71	0.15	-0.93	0.9266385

Note: Each plot below has left axis of log(h_{cor}) and bottom axis of log(v/v_{max})

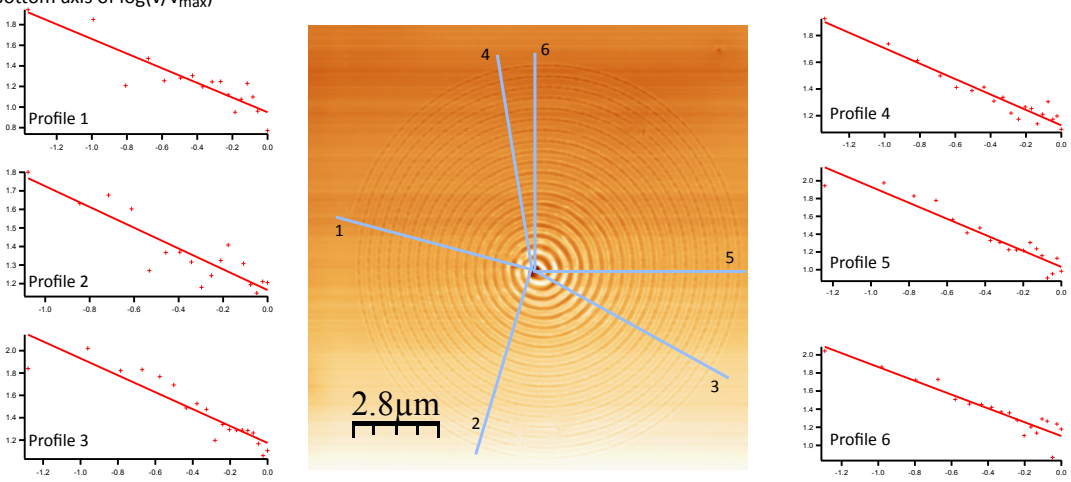

Figure S3. The data reported in a third data row of the Table 1 in the paper: PMMA heated at 97 ± 12 ^{o}C on the polymer surface.

Image	Material	R [μm]	T_{tip} [°C]	T_{surf} [°C]	T_{surf} Error	Profile #	overlap	Log (A)	Log (A) Error	-β	-β Error	V_Pr	Abs(V_Pr)
9DEC_3b	PMMA	6	206	97	12.5	1	100%	1.9019	0.0259	-0.17141	0.06	-0.587927	0.587927
9DEC_3b	PMMA	6	206	97	12.5	2	100%	2.0973	0.0298	0.0091003	0.07	0.035059	0.0350589
9DEC_3b	PMMA	6	206	97	12.5	3	100%	2.0726	0.0228	-0.029532	0.06	-0.130597	0.130597
9DEC_3b	PMMA	6	206	97	12.5	4	100%	1.9337	0.0241	-0.15959	0.06	-0.579352	0.579352
						AVERAGE	100%	2.00	0.10	-0.09	0.10	-0.32	0.3157043

Note: Each plot below has left axis of log(h_{cor}) and bottom axis of log(v/v_{max})

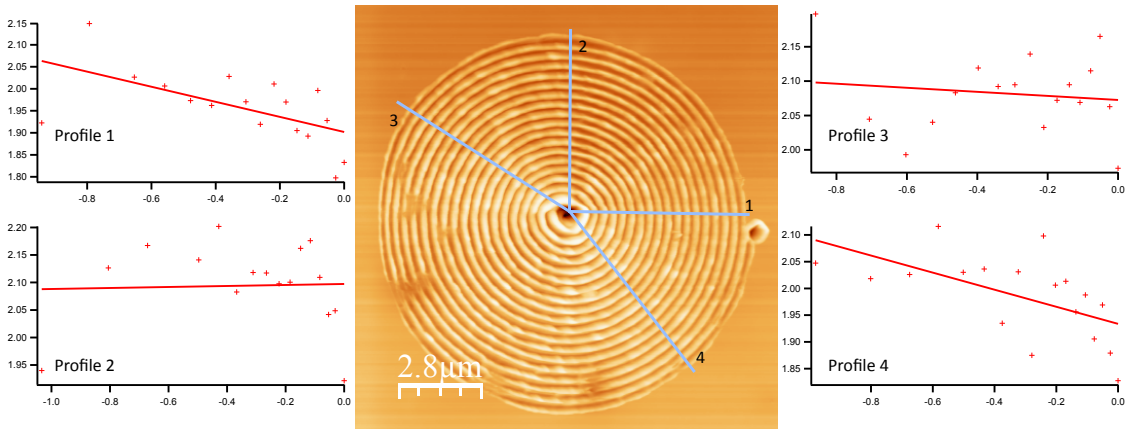

Figure S4. The data reported in a fourth data row of the Table 1 in the paper: PMMA heated at 97 ± 12 ^{o}C on the polymer surface.

Image	Material	R [μm]	T_{tip} [°C]	T_{surf} [°C]	T_{surf} Error	Profile #	overlap	Log (A)	Log (A) Error	-β	-β Error	V_Pr	Abs(V_Pr)
9DEC_0A	PMMA	6	247.0	113.4	13.9	1	100%	1.9561	0.0409	0.019821	0.1	0.053401	0.0534012
9DEC_0A	PMMA	6	247.0	113.4	13.9	2	100%	2.0124	0.0499	-0.047265	0.08	-0.141871	0.141871
9DEC_0A	PMMA	6	247.0	113.4	13.9	3	100%	1.9891	0.0526	-0.01878	0.13	-0.038015	0.0380153
9DEC_0A	PMMA	6	247.0	113.4	13.9	4	100%	2.108	0.0229	0.23888	0.05	0.767665	0.767665
						AVERAGE	100%	2.02	0.09	0.05	0.19	0.16	0.160295

Note: Each plot below has left axis of log(h_{cor}) and bottom axis of log(v/v_{max})

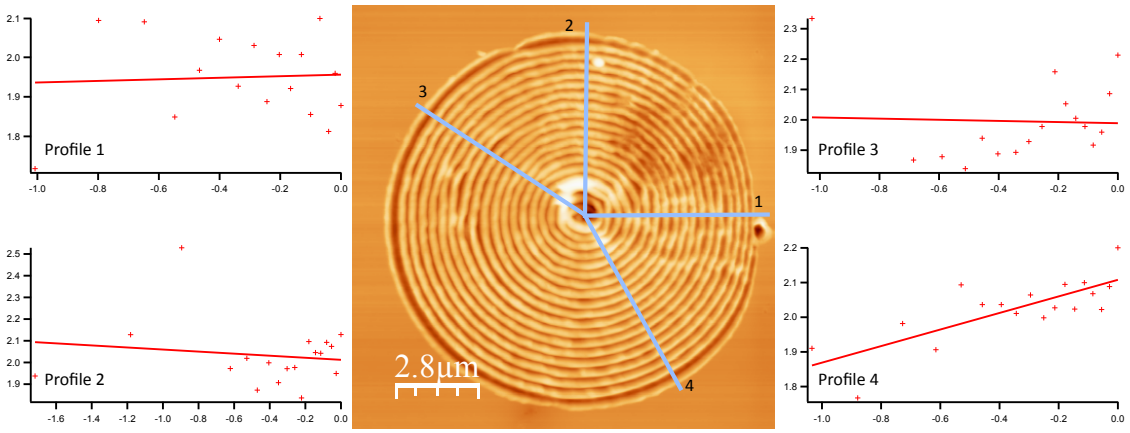

Figure S5. The data reported in a fifth data row of the Table 1 in the paper: PMMA heated at 113 ± 14 ^{o}C on the polymer surface.

Image	Material	R [µm]	T_{tip} [°C]	T_{surf} [°C]	T_{surf} Error	Profile #	overlap	Log (A)	Log (A) Error	-β	-β Error	V_Pr	Abs(V_Pr)
30DEC_89	PMMA	12	206	97	12.5	1	5%	1.1525	0.0462	-0.89613	0.09	-0.930723	0.930723
30DEC_89	PMMA	12	206	97	12.5	2	5%	1.6703	0.0304	-0.39025	0.05	-0.864873	0.864873
30DEC_89	PMMA	12	206	97	12.5	3	5%	1.4483	0.0476	-0.57311	0.09	-0.842035	0.842035
30DEC_89	PMMA	12	206	97	12.5	4	10%	1.3295	0.0516	-0.75043	0.09	-0.887183	0.887183
						AVERAGE	6%	1.40	0.27	-0.65	0.26	-0.88	0.8812035

Note: Each plot below has left axis of $\log(h_{cor})$ and bottom axis of $\log(v/v_{max})$

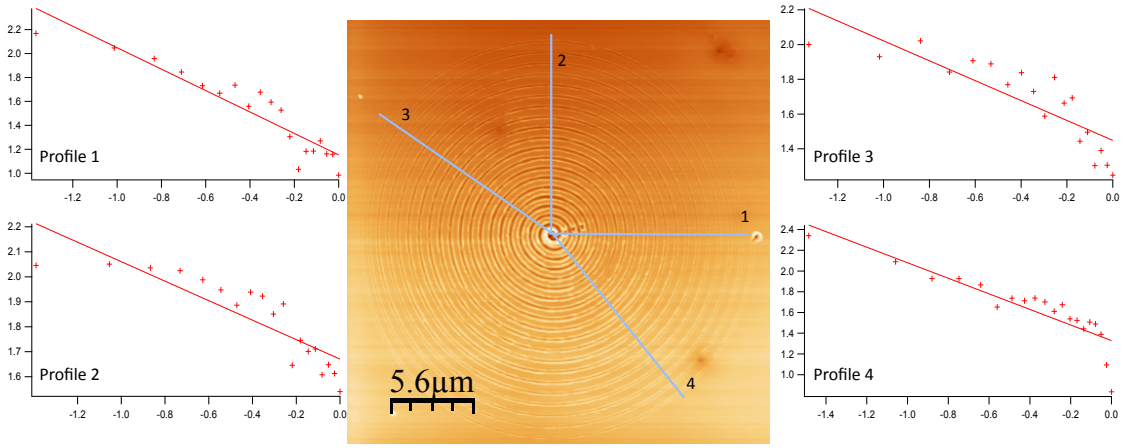

Figure S6. The data reported in a sixth data row of the Table 1 in the paper: PMMA heated at 97 ± 12 °C on the polymer surface; consecutive windings spaced by 600 nm.

Image	Material	R [µm]	T_{tip} [°C]	T_{surf} [°C]	T_{surf} Error	Profile #	overlap	Log (A)	Log (A) Error	-β	-β Error	V_Pr	Abs(V_Pr)
16JAN_77	PS	6	186	89.1	11.9	1	50%	1.3254	0.0474	-0.93472	0.1	-0.920082	0.920082
16JAN_77	PS	6	186	89.1	11.9	2	90%	1.8495	0.0245	-0.3055	0.05	-0.842797	0.842797
16JAN_77	PS	6	186	89.1	11.9	3	95%	1.8962	0.0419	-0.30428	0.08	-0.673372	0.673372
16JAN_77	PS	6	186	89.1	11.9	4	55%	1.6116	0.0362	-0.59964	0.08	-0.88001	0.88001
Note: Each plot below has left axis of log(h_{cor}) and bottom axis of log(v/v_{max})						AVERAGE	73%	1.67	0.23	-0.54	0.23	-0.83	0.8290653

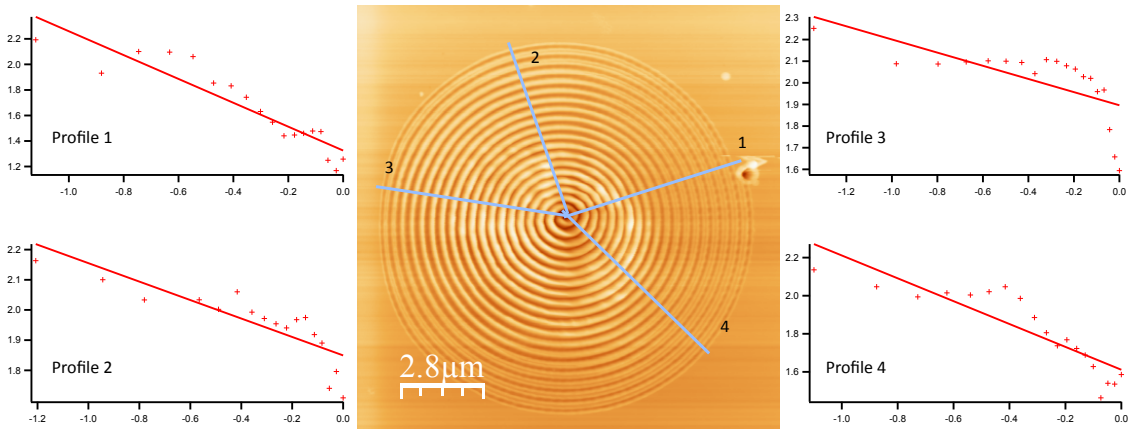

Figure S7. The data reported in a seventh data row of the Table 1 in the paper: PS heated at 89 ± 12 ^{o}C on the polymer surface.

Image	Material	R [µm]	T_{tip} [°C]	T_{surf} [°C]	T_{surf} Error	Profile #	overlap	Log (A)	Log (A) Error	-β	-β Error	V_Pr	Abs(V_Pr)
16JAN_5f	PS	12	207	96.7	12.5	1	15%	1.3824	0.0268	-0.9468	0.06	-0.972514	0.972514
16JAN_5f	PS	12	207	96.7	12.5	2	40%	1.8978	0.0165	-0.56035	0.03	-0.972944	0.972944
16JAN_5f	PS	12	207	96.7	12.5	3	35%	1.9504	0.0176	-0.42166	0.04	-0.943776	0.943776
16JAN_5f	PS	12	207	96.7	12.5	4	20%	1.5803	0.0232	-0.80889	0.05	-0.966927	0.966927
Note: Each plot below has left axis of log(h_{cor}) and bottom axis of log(v/v_{max})						AVERAGE	28%	1.70	0.25	-0.68	0.26	-0.96	0.9640403

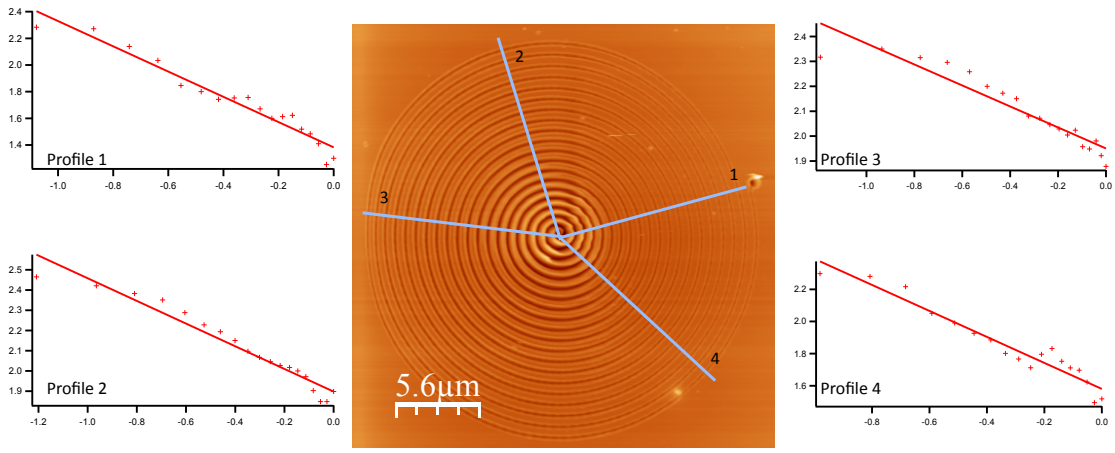

Figure S8. The data reported in a eight data row of the Table 1 in the paper: PS heated at 97 ± 12 °C on the polymer surface; consecutive windings spaced by 600 nm.

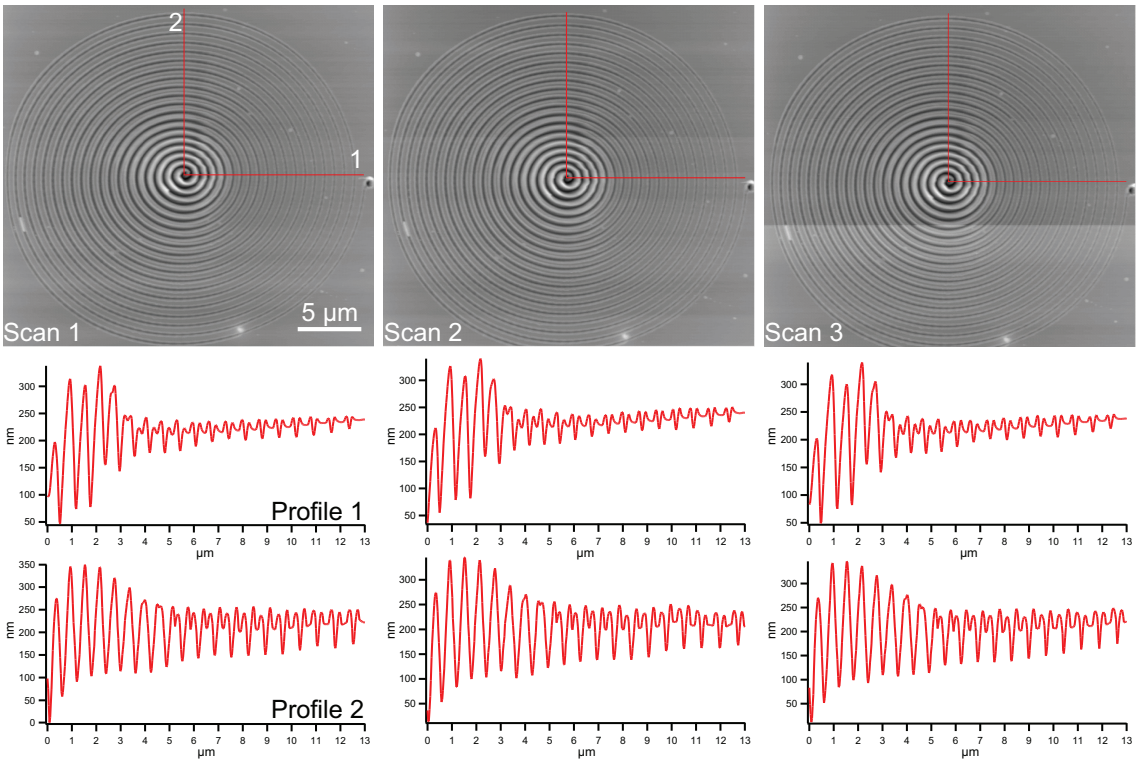

Figure S9. Three subsequent rescans of a given spiral on a PS polymer surface along with two cross-sections visualized for each rescan. For rescanning, a regular MLCT-F cantilever from Bruker at 15 ± 3 nN contact force was used, as in the main paper. These images attest that spiral damage produced by MLCT-F rescans is negligible. The original spiral was obtained with a thermal cantilever at a tip-sample interface temperature of 97 ± 13 degr C.

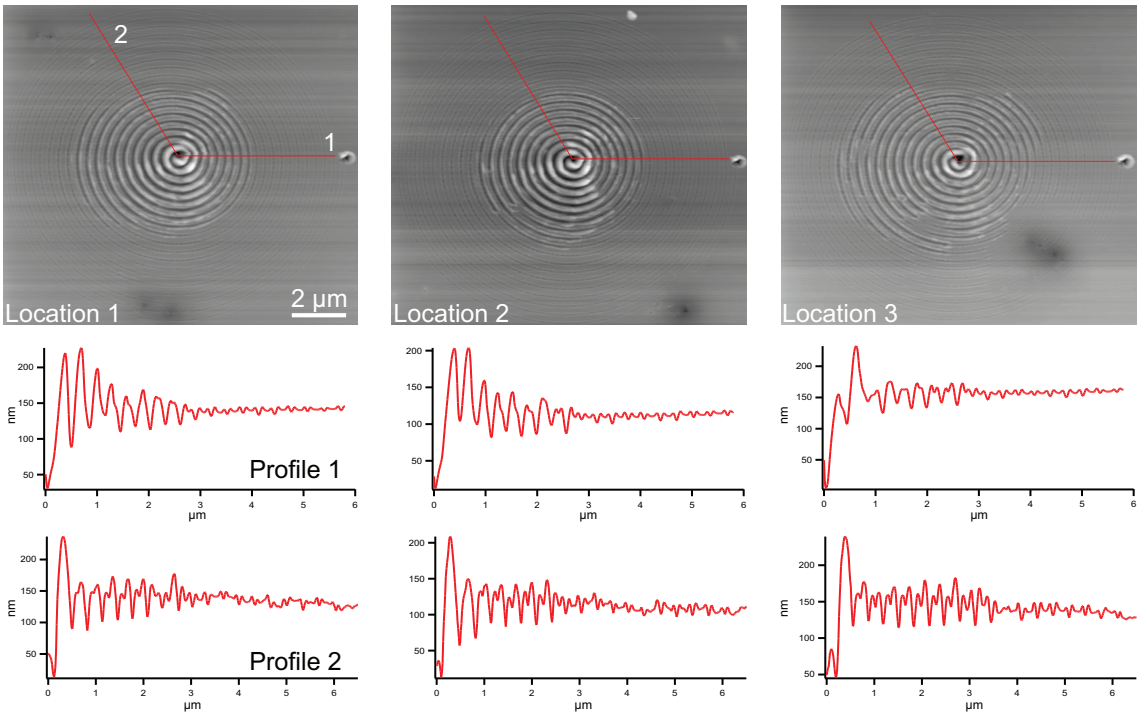

Figure S10. Assessment of spatial heterogeneity for corrugation profiles on PMMA. A particular spiral was created at three very different spatial location, but at very similar conditions of a tip-sample interface temperature of 97 ± 13 degr C.

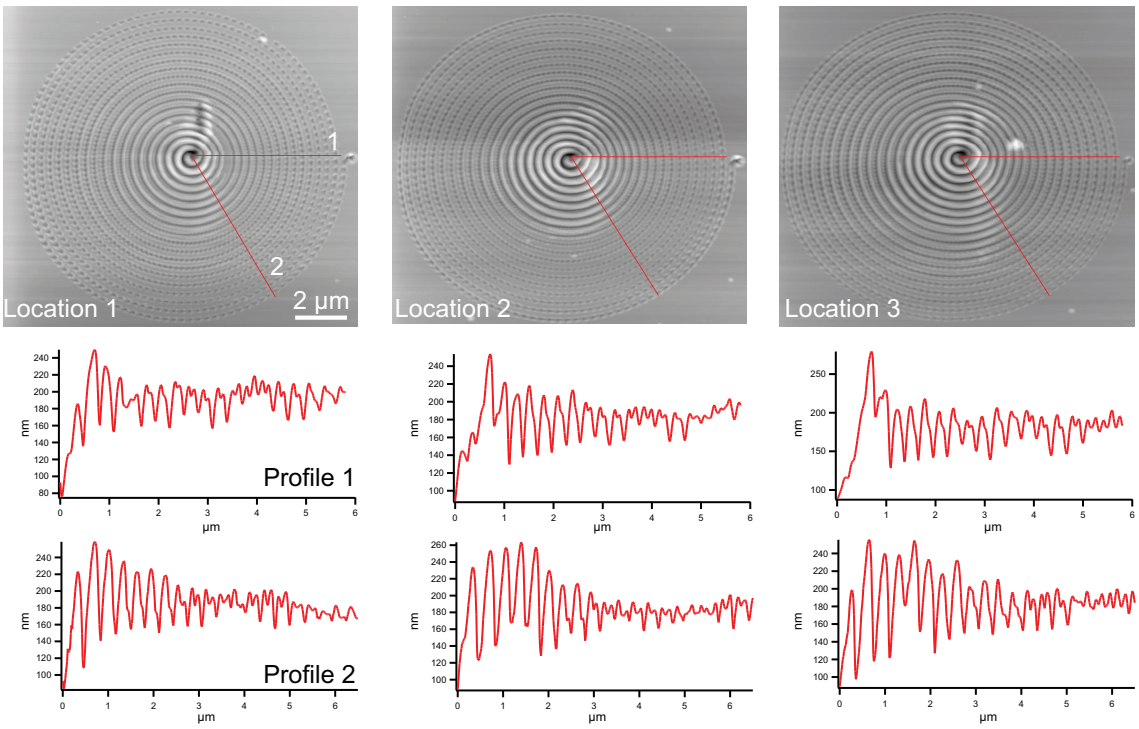

Figure S11. Assessment of spatial heterogeneity for corrugation profiles on PS. A particular spiral was created at three very different spatial location, but at very similar conditions of a tip-sample interface temperature of 97 ± 13 degr C.